ELSEVIER

Catalysis Today 65 (2001) 77–89

CATALYSIS TODAY

www.elsevier.com/locate/cattod

The role of Pd precursors in the oxidation of carbon monoxide over Pd/Al_2O_3 and $Pd/CeO_2/Al_2O_3$ catalysts

Robson S. Monteiro[1], Lídia C. Dieguez, Martin Schmal*

NUCAT/PEQ/COPPE and Escola de Química, Federal University of Rio de Janeiro, Caixa Postal 68502, CEP 21945-970, Rio de Janeiro, Brazil

Abstract

The role of palladium precursors (e.g. chloride — $PdCl_2$; acetylacetonate — $Pd(acac)_2$; nitrate — $Pd(NO_3)_2$) in the catalytic properties of Pd/Al_2O_3 and $Pd/CeO_2/Al_2O_3$ catalysts toward CO oxidation was herein investigated. The characterization techniques used for mapping the Pd sites were H_2 and CO chemisorption, infrared spectroscopy (FTIR) of CO adsorbed, and temperature-programmed desorption (TPD). Unsteady-state CO oxidation was carried out by temperature-programmed surface reaction (TPSR). The nature of palladium precursors and their interaction with CeO_2 affected the metallic dispersion and the site morphologies. Highly dispersed metal particles ($d > 50\%$) were obtained by using palladium chloride and acetylacetonate precursors on Pd/Al_2O_3 catalysts. Pd(1 0 0) and Pd(1 1 1) were the major palladium crystallite orientations in these samples, but a larger amount of low coordination sites located on Pd(1 0 0) faces was observed for the ex-chloride sample. These sites accounted for the oxidation of CO at very low temperatures on Pd-Cl catalyst. In the presence of ceria, the Pd dispersion was a function of the way in which each Pd precursors interacted with CeO_2. A two-fold decrease of dispersion was obtained to ex-chloride sample, while a two-fold increase to ex-nitrate and the same dispersion to ex-acetylacetonate samples were otherwise observed. The metallic redispersion may be the result of the occupancy of ceria oxygen vacancies by the palladium crystallites. Ultimately, the interaction with ceria redispersed Pd crystallites in a more organized bi-dimensional structure with the predominance of (1 1 1) orientation. Due to the transient conditions of the reaction, ceria did not promote, as expected, the oxidation of CO. Ceria reduced species (Ce^{3+}) were not able to help CO oxidize at lower temperatures due to lack of oxygen into its lattice. Thus, the highest rates for CO oxidation were only observed at higher temperatures for the $Pd/CeO_2/Al_2O_3$ catalysts, a result of a combination of strong competition for oxygen molecules, which have replenished the ceria lattice, and the low activity of Pd(1 1 1) sites.

Keywords: Unsteady-state oxidation of CO; Palladium; Cerium oxide; Pd–Ce interaction; Pd precursors

1. Introduction

Carbon monoxide oxidation on platinum metal group has been widely studied due to its extensive use in pollution control devices, such as catalytic converters and gas sensors [1,2]. Early studies [3,4] have reported that the oxidation of CO on palladium surfaces is a structure-insensitive reaction and proceeds through a Langmuir–Hinshelwood kinetic. Reaction rates are affected by CO coverage, showing an inverse first-order dependence on CO concentration. More recently, Haruta et al. [5] reported that highly dispersed gold deposited on reducible metal oxides has a remarkable activity for CO oxidation at low tempera-

* Corresponding author. Tel.: +55-21-590-2241; fax: +55-21-290-6626.
E-mail address: schmal@peq.coppe.ufrj.br (M. Schmal).
[1] Present address: Department of Chemical Engineering, Worcester Polytechnic Institute, 100 Institute Road, Worcester, MA 01609, USA.

0920-5861/01/$ – see front matter
PII: S0920-5861(00)00547-2

tures, and the reaction was independent on the partial pressures of CO and O_2 and structure sensitive. Exploring the possibilities of metal–support interaction by changing Pd site properties toward CO oxidation, Pavlova et al. [6,7] have also observed structure sensitivity at low temperatures on small ensembles of Pd supported over Al_2O_3, TiO_2 and SiO_2 carriers.

Palladium active sites are influenced by several factors, as including the particle mean size, the support interaction, the nature of precursor salts utilized in the preparation, and so forth. The particle size plays an important role for structure-sensitive reactions since either the site coordination, such as kink, step, and terrace atoms, or the crystal orientation affect the catalytic reactivity [8]. The metal–support interaction also contributes to change Pd sites, especially when they are supported on reducible transition metal oxides (TiO_2, CeO_2, Nb_2O_5 and La_2O_3). Epitaxial alignment with restructuring of catalytic sites at the interface, electronic transfer or encapsulation of metal particles by reduced support species, are some of the explanations that are possible to find in literature to define metal–support interaction nature [9–11].

In this study the nature of Pd active sites on Pd/Al_2O_3 and $Pd/CeO_2/Al_2O_3$ catalysts was investigated. The main goals were to determine whether different Pd precursors interact distinctively with CeO_2, and to understand how the interaction mechanism affects the Pd catalytic properties for CO oxidation. The palladium sites were characterized by H_2 and CO chemisorption, temperature-programmed desorption (TPD), and infrared spectroscopy (FTIR) of CO adsorbed. The probing reaction was the oxidation of carbon monoxide carried out under transient conditions by temperature-programmed surface reaction (TPSR).

2. Experimental methods

2.1. Preparation of catalysts

Catalysts with 1 wt.% Pd were prepared by impregnation over either γ-Al_2O_3 (BET area of 208 $m^2\,g^{-1}$) or CeO_2/Al_2O_3 (BET area of 193 $m^2\,g^{-1}$) carriers. The γ-Al_2O_3 (AL-3916P, Engelhard Corp.) was previously calcined at 823 K for 16 h in an aerated muffle at a heating rate of 2 K min^{-1}. The CeO_2/Al_2O_3 system was prepared from the grafting reaction between a cerium acetylacetonate precursor — $Ce(acac)_3$ (Aldrich Co.) — and alumina surface hydroxyl groups as described elsewhere [12]. The grafting reaction, carried out in six successive steps, had the objective of increasing the preparation efficiency in order to obtain well-dispersed ceria particles closer to the theoretical monolayer (~18–20 wt.% CeO_2). This methodology allowed to cover at least 66% of the alumina surface with ceria [13]. The measurement of CeO_2 dispersion was based on the method developed by Johnson and Mooi [14], in which the H_2 uptake assigned to the reduction of CeO_2 capping oxygen and calculated by TPR analysis is correlated to the surface area of the CeO_2. A conversion factor of 4.2 μmol $H_2\,m^{-2}$ CeO_2 [15] calculated by using catalysts with different loadings of ceria was used to measure the surface area of the CeO_2 (127 $m^2\,g^{-1}$) [13]. Thus, CeO_2 coverage was obtained by calculating the ratio of CeO_2 surface area and the BET area of CeO_2/Al_2O_3. The Pd precursors utilized were $PdCl_2$ (Aldrich, 99.999%), $Pd(NO_3)_2$ (Aldrich) and $Pd(acac)_2$ (Aldrich, 99%). Aqueous acid solutions of 1:1, either HCl or HNO_3, were used to dissolve $PdCl_2$ or $Pd(NO_3)_2$, followed by heating in order to evaporate chloride and nitrate residues. The solution volume for incipient wetness impregnation was the same for the pore volume of the support. Toluene (Vetec, 99%) was used to dissolve $Pd(acac)_2$ and wet impregnation was carried out at room temperature for 24 h, followed by filtration. After impregnation the catalysts were dried in a muffle at 393 K for 18 h, followed by calcination in an aerated muffle at 773 K for 4 h. Pd-X or PdCe-X (X means Cl, acac or N) was used to denote Pd/Al_2O_3 or $Pd/CeO_2/Al_2O_3$ catalysts prepared by chloride, acetylacetonate or nitrate precursors.

2.2. Characterization techniques

H_2 and CO chemisorption measurements were made using volumetric and pulse techniques. Volumetric chemisorption was carried out in the ASAP 2000C Micromeritics equipment, where Pd/Al_2O_3 and $Pd/CeO_2/Al_2O_3$ were pretreated before the adsorption. Pd/Al_2O_3 catalysts were dried at 423 K for 30 min under Ar flow (30 ml min^{-1}). Aiming for the elimination of likely carbonate species adsorbed on the CeO_2 surface due to its exposure to atmosphere

[16], the $Pd/CeO_2/Al_2O_3$ catalysts were treated under a flow of 5% O_2/He (50 ml min^{-1}) at 673 K for 60 min, followed by flowing Ar (50 ml min^{-1}) at 773 K for 90 min. The samples were then reduced by flowing H_2 (50 ml min^{-1}) at a heating rate of 10 K min^{-1} from room temperature to 773 K. After reduction, the samples were evacuated for 1 h at reduction temperature (773 K) and cooled down to adsorption temperature under a vacuum. Irreversible uptakes were determined from dual isotherm measurements for hydrogen at 343 K and carbon monoxide at room temperature, according to the methodology described by Benson et al. [17] and Yates and Sinfelt [18] for H_2 and CO, respectively. H_2 or CO pulses of 1.6 cm^3 from 1.7% H_2/Ar or 5% CO/He mixtures on reduced samples were monitored by a quadrupole mass spectrometer, and the saturation peak corresponding to the maximum amount of gas admitted in the quadrupolar chamber was used to quantify thermal desorption peaks. Metallic dispersion was calculated using hydrogen chemisorption and assuming a stoichiometric ratio $H/Pd = 1$. Following CO pulses, the temperature-programmed desorption (TPD) was performed by heating the samples at 20 K min^{-1} from room temperature to 773 K under argon flow (50 ml min^{-1}). Masses (*m*/*e*: 2, 16, 18, 28, 32 and 44) were monitored during TPD, and the species observed were quantified by prior injections of known amounts of gases.

Infrared spectroscopy (FTIR) of adsorbed carbon monoxide was carried out on self-supported samples compressed into thin disk wafers with a 20 mm diameter. The disk was placed in a sample holder and introduced into a cell, which allowed in situ reduction. After the pretreatment and reduction described earlier, the samples were evacuated at reduction temperature for 1 h prior to cooling down to room temperature. Then, 30 Torr (1 Torr = 133.3 Pa) of CO was adsorbed at room temperature. After the evacuation at room temperature for 1 h, IR spectra were recorded on a FTIR Perkin-Elmer 2000 spectrometer.

2.3. Oxidation of carbon monoxide

Carbon monoxide oxidation was performed under transient conditions by a temperature-programmed surface reaction (TPSR) in a tubular flow reactor at atmospheric pressure. $Pd/CeO_2/Al_2O_3$ catalysts were treated under flow of 0.5% O_2/He (50 ml min^{-1}) at 673 K for 60 min following flow of Ar (50 ml min^{-1}) at 773 K for 90 min. Pd/Al_2O_3 catalysts, in turn, were dried at 423 K for 30 min under Ar flow (30 ml min^{-1}). The samples were then reduced by flowing H_2 (50 ml min^{-1}) at a heating rate of 10 K min^{-1} from room temperature to 773 K. Initial adsorption of CO on reduced surfaces was made by pulses of 5% CO/He at room temperature until reaches the saturation. After CO pulses, a flow of 0.5% O_2/He (25 ml min^{-1}) diluted in Ar (25 ml min^{-1}) was introduced into the reactor. Initially, the dead volume of the reactor was observed, followed by O_2 uptake at room temperature before the reactor was heated at 20 K min^{-1} from room temperature to 773 K. A quadrupole mass spectrometer (Balzers, PRISMA) coupled to an analytical control system (Dycor-QGA, Ametek) was used to record signal intensity of different masses previously chosen (*m*/*e*: 2, 16, 18, 28, 32, and 44) during TPSR. Pulses of CO_2 and O_2 were made after ending each run to calibrate CO_2 and O_2 concentrations.

3. Results and discussion

3.1. Pd sites mapping

3.1.1. Metallic dispersion

Table 1 shows CO chemisorption and metallic dispersion measured by H_2 adsorption using volumetric and pulse techniques. No significant changing in the chemisorption values were found in either method. The influence of Pd precursors in the metallic dispersion of the catalysts is very clear. Pd-Cl and Pd-acac samples showed the same dispersion values (∼51%), well above of the value obtained for Pd-N sample (∼16%). Chloride and acetylacetonate precursors are known for interacting with hydroxyl groups present on the surface of alumina leading to a good distribution of the metallic particles [12]. In the case of chloride precursors, the formation of Pd oxychloride species ($Pd_xO_yCl_z$) would be responsible for the high dispersion and for keeping it under harsh conditions as well [19–21]. On the other side, lack of interaction with OH groups by nitrate precursors would promote coalescence of Pd particles.

CO/H_2 molar ratios showed that the stoichiometry of CO chemisorption on Pd sites was in between the linear-bonded form ($CO/H_2 = 2$) and bridged-bonded

Table 1
Results of H_2 and CO chemisorption by using volumetric and pulse techniques

Sample	Metallic content (%)	Volumetric chemisorption				Pulse chemisorption			
		H_2 (μmol mg^{-1} Pd)	CO (μmol mg^{-1} Pd)	CO/H_2 ratio	$D_{H_2,v}$[a] (%)	H_2 (μmol mg^{-1} Pd)	CO (μmol mg^{-1} Pd)	CO/H_2 ratio	$D_{H_2,p}$[a] (%)
Pd-Cl	0.99	2.38	3.46	1.45	51	2.57	3.66	1.42	54
Pd-acac	0.94	2.39	4.57	1.91	51	2.48	4.32	1.74	53
Pd-N	1.04	0.74	1.01	1.37	16	0.82	1.06	1.29	17
PdCe-Cl	0.91	1.19	1.73	1.45	25	1.23	1.74	1.41	26
PdCe-acac	0.93	2.36	4.61	1.95	50	2.23	3.88	1.74	47
PdCe-N	0.99	1.72	1.83	1.06	37	1.99	2.59	1.30	42

[a] $D_{H_2,v}$ and $D_{H_2,p}$ metallic dispersion measured by H_2 chemisorption, volumetric (v) and pulse (p) techniques.

form ($CO/H_2 = 1$) for all Pd/Al_2O_3 catalysts. However, the Pd-acac catalyst presented a CO/H_2 ratio close to 2, which means that the CO was adsorbed preferentially in linear-bonded form for this catalyst. A more detailed discussion about the role of CO adsorbed species in the mapping of Pd sites will be further given by FTIR and TPD analyses.

In the presence of CeO_2, H_2 chemisorption showed a behavior quite interesting. The metallic dispersion was two-fold lower for the PdCe-Cl catalyst, the same for the PdCe-acac catalyst and two-fold higher for the PdCe-N catalyst in comparison with their counterparts with no ceria. These results show that the Pd precursors have interacted distinctively with the CeO_2/Al_2O_3 system. Monteiro et al. [22] observed that the metallic dispersion decreased for Al_2O_3-supported Pd-CeO_2 catalysts prepared by chloride precursors. The authors attributed this phenomenon to the decoration of Pd sites by CeO_x species reduced at the Pd–Ce interface. Nevertheless, the question raised is why does only PdCe-Cl catalyst dispersion decrease? Should not the others catalysts follow the same trend?

Vacancy model proposed by Sanchez and Gazquez [10] foresees high metallic dispersion for Pd, Pt and Rh metals supported on fluorite-type oxides (e.g. CeO_2) with good resistance to sintering. In this model, oxygen-deficient vacancies on the surface of ceria would accommodate Pd crystallites in their structure leading to a more dispersed state. Datye et al. [23] and Kalakkad et al. [24] have reported in studies of transmission electron microscopy of Pt/CeO_2 catalysts reduced at high temperature evidence of an epitaxial alignment between ceria anionic vacancies and dispersed Pt crystallites. No decoration of Pt sites by CeO_x species was observed. In contrast with data reported for noble metals (NM) supported on TiO_2, Bernal et al. [11] observed by HREM studies that metal decoration on NM/CeO_2 catalysts is not a relevant factor on samples reduced at 773 K or lower temperatures. Thus, Pd–Ce interaction would then be promoted by ceria species in its reduced state (Ce^{3+}). This interaction could yet inhibit the metal agglomeration on the surface, contributing to either its redispersion or maintenance of a highly dispersed state.

Considering the studies mentioned earlier, it seems that the low dispersion obtained for the PdCe-Cl catalyst is straightforwardly related to a weaker Pd–Ce interaction. In this case, the likely existence of chlorine residues on the catalyst surface might inhibit this desirable interaction. Moreover, chloride precursors would not find great availability of OH groups due to the good coverage of alumina by ceria species (∼66%) and as a result the Pd particles would agglomerate and grow.

Several authors have described the possibility of chlorine residues to influence metal–support interaction in CeO_2-based catalysts [25–27]. Chlorine (Cl^-) leftovers are hard to eliminate from the surface when metal chloride precursors are used in the preparation of catalysts. On a reduced surface of the ceria (Ce^{3+}), Cl^- anions are strongly bound at the support surface due to the strong interactions of Cl^- with Ce^{3+} ions formed during the reduction process. This interaction could lead to the formation of stable CeOCl species on the ceria surface [27]. According to Kepinski and Wolcyrz [28] chlorine residues react with ceria at 770 and 870 K to form ribbon-like CeOCl crystals and their

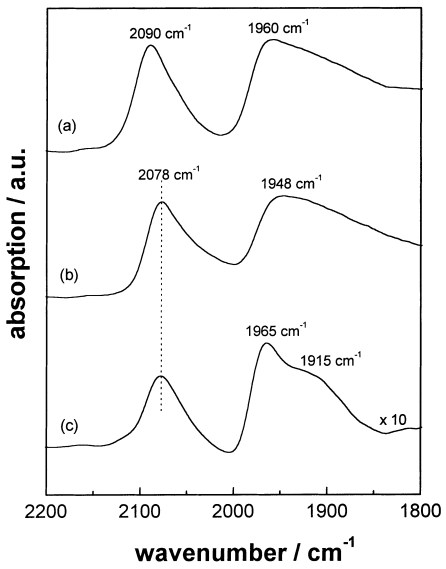

Fig. 1. Infrared spectra for Pd/Al_2O_3 catalysts: (a) Pd-Cl; (b) Pd-acac; and (c) Pd-N. A complete monolayer of CO ($\theta = 1$) was obtained for all samples.

formation is a possible mechanism of the deactivation of ceria-promoted Pd/SiO_2 catalysts. As a consequence, Pd–Ce interaction would be very weak with significant effects on Pd particle size distribution [29].

3.1.2. FTIR of CO adsorbed

Infrared spectroscopy of CO adsorbed on reduced surfaces of Pd-Cl, Pd-acac and Pd-N catalysts are presented in Fig. 1. Two major peaks that have been commonly attributed to linearly-bonded CO (above 2000 cm^{-1}) and bridged-bonded CO (below 2000 cm^{-1}) were observed [30–32]. For the Pd-Cl catalyst, the frequency of CO linear at 2090 cm^{-1} was higher than the frequency observed at 2078 cm^{-1} for Pd-acac and Pd-N catalysts. It is noteworthy to mention that the higher intensity of CO linear species for Pd-Cl and Pd-acac catalysts are in agreement with the high metallic dispersion observed in these samples. A broad band at higher frequency (1960 cm^{-1}) was also observed for bridged-bonded CO on Pd-Cl catalyst in comparison with that at 1948 cm^{-1} for the Pd-acac catalyst. Besides a bridged-bonded CO at 1965 cm^{-1}, a lower frequency for CO bridged species was also observed at 1915 cm^{-1} for the Pd-N catalyst.

The difference in the position of CO absorption frequencies demonstrates clearly that the nature of Pd precursors play a role in the Pd site properties. As described earlier, the precursor–support interaction influences the Pd particle size distribution, which determines the nature of sites available on the surface. On surfaces with a predominance of low coordination sites, an infrared C–O stretching frequency is expected at higher frequencies. Conversely, the C–O absorption frequency should be lowered when high coordination sites faces are present. This behavior is associated with the electron transfer from the metal to the adsorbed CO molecule. According to Blyholder [33], in the low coordination sites the electron availability to back-donate from the filled palladium d orbital to the $2\pi^*$-antibonding vacant orbital of CO is smaller than that on the high coordination sites, due to the competition with adjacent atoms. Thus, on sites of low coordination number, the Pd–CO bond is weaker than on sites of high coordination number, which means that C–O bonding is strengthened with absorption of infrared bands located at higher frequencies.

A possibility of linking IR reflection–absorption results of CO adsorbed on single crystals of various orientations [34,35] with those obtained on supported Pd was reported by Palazov et al. [36]. According to these studies, at high coverage of CO ($\theta > 0.5$), the bands of bridged-bonded CO are located at higher frequencies on Pd(1 0 0) planes when compared with Pd(1 1 1) planes. The difference of metallic coordination between Pd(1 0 0) and Pd(1 1 1) planes accounts for this behavior.

Even though Pd-Cl and Pd-acac catalysts have had the same metallic dispersion, FTIR data showed that the nature of Pd sites is different. CO absorption at higher frequencies observed for Pd-Cl catalyst indicates that the Pd sites are mainly of low coordination with (1 0 0) orientation while CO absorption at lower frequencies for Pd-acac catalyst suggests high coordination sites with (1 1 1) orientation. Metallic coordination states the difference in the density of sites with edges and corners, and such imperfections are important in the band positions of CO adsorbed. Thus, it is likely that a higher density of edges and corners sort of sites would be found on the Pd-Cl catalyst than on the Pd-acac catalyst due to the difference of crystal orientation.

For the Pd-N catalyst, two species of bridged-bonded CO were observed at 1965 and 1915 cm^{-1} and according to the assignments described earlier would be, respectively, CO bonded on the (1 0 0) and the (1 1 1) faces. However, on samples with low dispersion, the higher CO bridged frequencies could be also attributed to compressed-bridged species, i.e. bridged carbonyls in direct interaction. FTIR studies carried out by Tessier et al. [37] on ex-nitrate samples of Pd/Al_2O_3 catalysts suggest that this interaction should be stronger due to the low dispersion, allowing numerous CO neighbors to be coupled. This assignment seems to be more appropriate for bridged-bonded CO at 1965 cm^{-1} since the Pd-N catalyst showed the lowest dispersion among the catalysts studied. As the proportion of Pd(1 1 1) sites relative to Pd(1 0 0) sites increases with decreasing dispersion [38], Pd(1 1 1) may be the dominant orientation on the Pd-N catalyst. Another possibility to explain the high frequency absorption of CO is the increase of high-index sites.

Fig. 2 shows that the presence of CeO_2 has changed significantly the FTIR spectra for $Pd/CeO_2/Al_2O_3$ catalysts. The intensity of CO absorption peaks for PdCe-Cl and PdCe-N catalysts followed the metallic dispersion behavior with decreasing for ex-chloride and increasing for ex-nitrate samples. However, it was not only the intensity of the peaks that changed, the positions were also shifted as a result of Pd–Ce interaction.

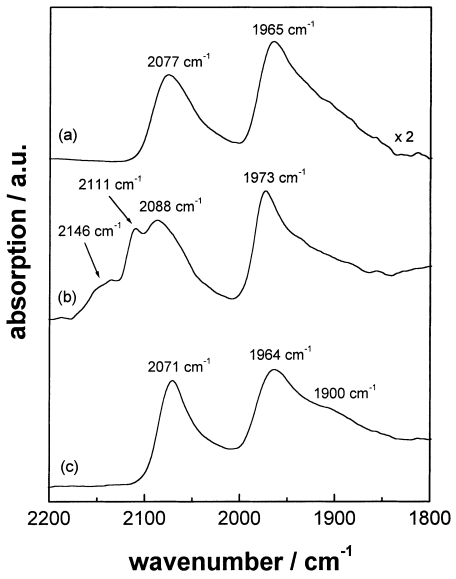

Fig. 2. Infrared spectra for $Pd/CeO_2/Al_2O_3$ catalysts: (a) PdCe-Cl; (b) PdCe-acac; and (c) PdCe-N. A complete monolayer of CO ($\theta = 1$) was obtained for all samples.

The PdCe-Cl catalyst lowered the frequency of linearly-bonded CO (2077 cm^{-1}), and its CO bridged-band is sharper than that observed for the Pd-Cl catalyst. An increasing of bridge-to-linear ratio suggests a decrease in the metallic dispersion. Its profile resembles that observed for low-dispersed Pd-N catalyst. Like the Pd-N catalyst, the nature of Pd sites for the PdCe-Cl catalyst should be Pd(1 1 1) faces.

For the PdCe-acac catalyst, the changes in the infrared spectra were significant in comparison with the Pd-acac catalyst. Besides CO linearly (2090 cm^{-1}) and bridged (1973 cm^{-1}) bonded two new bands arose in frequencies higher than 2100 cm^{-1}. These bands can be attributed to CO adsorbed on cationic species of palladium. Thus, the band at 2111 cm^{-1} is assigned to CO linear on Pd^{+}, and the band at 2146 cm^{-1}, to CO linear on Pd^{2+} [37]. The existence of electron-deficient Pd species in the presence of ceria has been reported by Shyu et al. [39] and Sass et al. [40]. These authors have postulated a Pd–Ce interaction model in which Pd^{+}. O_2^{-} species would be formed at the interface. However, the presence of Pd^{2+} cation is very surprisingly suggesting an incomplete reduction of PdO species. Ceria is a strong oxidizing agent and its interaction with palladium could keep it in a more oxidized state even on reducing environments. This behavior presented by the PdCe-acac catalyst reinsures that the precursor nature plays an important role in the Pd–Ce interaction, which was far more intense for ex-acetylacetonate catalyst.

In regard to the PdCe-N catalyst, the infrared spectrum did not change so much, despite the dispersion increase reported. The signal intensity is higher than the Pd-N catalyst with noticeable increase in the CO linear peak. However, the CO linear and bridged species showed the same absorption frequencies, respectively, at 2071, 1964 and 1900 cm^{-1}. In this sample, the Pd–Ce interaction contributed to spreading out Pd particles without modifying the site morphology. Thus, Pd(1 1 1) faces are also the main orientation for PdCe-N catalyst.

The epitaxial alignment between ceria anionic vacancies and Pd dispersed crystallites, which was postulated to explain the metallic dispersion, clearly led

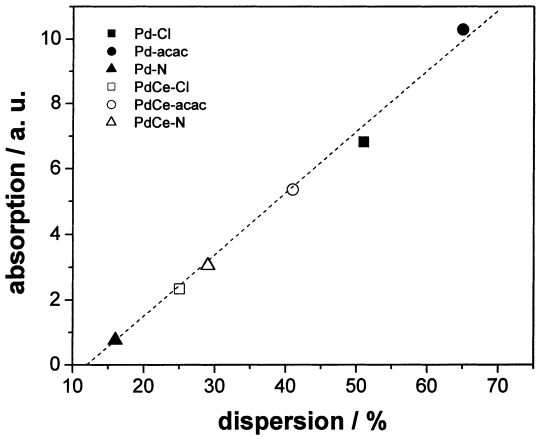

Fig. 3. Linear relationship between CO total absorption obtained from FTIR spectra and Pd metallic dispersion.

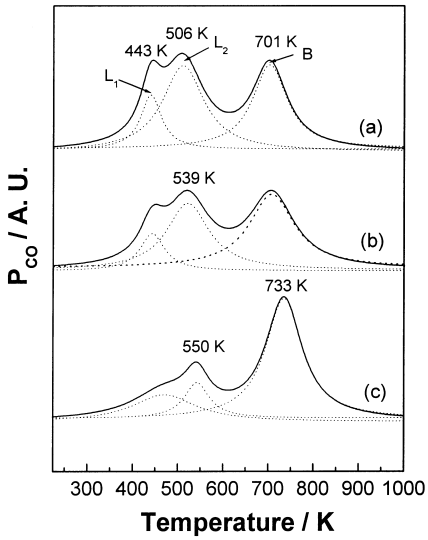

Fig. 4. TPD profiles for Pd/Al_2O_3 catalysts: (a) Pd-Cl; (b) Pd-acac; and (c) Pd-N.

to changing the nature of Pd sites. In these catalysts, Pd(1 1 1) faces were favored in detriment of Pd(1 0 0) faces, and bridged-bonded CO is the major species. According to Badri et al. [41], Pd particles highly dispersed over a high-surface area ceria support would form a raft-structure, mainly two-dimensional, looking like (1 1 1) planes and possibly have a disorganized part. Ultimately, the interaction with ceria favors the redispersion of Pd crystallites in a more organized bi-dimensional structure with the predominance of Pd(1 1 1) orientation.

In order to ensure the dispersion of the catalysts measured by H_2 chemisorption, the same methodology developed by Duplan and Praliaud [42] was used in this work. Basically, these authors have established a linear relationship between total CO absorption and metallic dispersion of Pd/Al_2O_3 catalysts, which is obtained by hydrogen chemisorption. This linear relation allowed them to estimate the metallic dispersion on $Pd/CeO_2/Al_2O_3$ catalysts. Fig. 3 shows the linear plot obtained to the samples prepared in this study. The results fairly agree with those observed in the chemisorption measurements. High dispersion values were observed for Pd-acac, Pd-Cl and PdCe-acac catalysts. PdCe-Cl dispersion decrease and redispersion for PdCe-N catalysts were also verified. Therefore, it is evident that the palladium precursors and their interaction with ceria greatly affected the distribution and properties of Pd sites on Pd/Al_2O_3 and $Pd/CeO_2/Al_2O_3$ catalysts.

3.1.3. Thermal desorption of CO

TPD experiments were performed following the CO pulse adsorption measurements and the results are shown in Fig. 4. The data indicates a diversity of adsorption sites for CO on Pd as well as variation in the proportion and distribution of CO species. Pd-Cl and Pd-acac catalysts showed similar behavior with three peaks at 443, 506 and 701 K, while for the Pd-N catalyst the desorption of these peaks were slightly shifted to higher temperatures. According to Rieck and Bell [38,43], the adsorption states of CO molecules on a Pd surface can be associated to the two species of CO (linear and bridged-bonded) previously identified on FTIR-based studies and adsorbed on Pd sites with different surface morphologies.

From this standpoint and based on infrared results (Figs. 1 and 2), one could attribute the two peaks at low temperatures (<600 K) to linear-bonded CO, and the peak at high temperature (>600 K) to bridged-bonded CO. The distribution of these species change as Pd precursors change as well, as it is shown in Table 2. Such behavior is assigned to the morphological differences of the Pd sites. Thus, L_1 and L_2 stand for linearly-bonded CO on Pd(1 0 0) and Pd(1 1 1) planes, respectively, while B for bridged-bonded species on Pd(1 1 1) plane. The absence of bridged-bonded CO

Table 2
Distribution and relative proportion of adsorbed CO species from TPD profiles

Sample	CO linear[a] (Torr s^{-1})		L_1/L_2 ratio	CO bridged[b] (Torr s^{-1})	B/L ratio[c]
	$L_1 \times 10^8$	$L_2 \times 10^8$		$B \times 10^8$	
Pd-Cl	4.92	14.03	0.35	12.20	0.64
Pd-acac	1.79	14.08	0.13	13.17	0.83
Pd-N	0.90	4.57	0.19	18.19	4.42
PdCe-Cl	3.05	8.64	0.35	20.15	1.72
PdCe-acac	–	1.34	–	13.63	1.32
PdCe-N	–	4.08	–	17.35	4.25

[a] L_1 and L_2 are the linearly bonded CO on Pd(1 0 0) and Pd(1 1 1) faces, respectively.
[b] B is the bridged-bonded CO.
[c] $L = L_1 + L_2$.

on the Pd(1 0 0) plane is due to its role in CO disproportionation observed and described below. A larger bridge-to-linear ratio (B/L) for the Pd-N catalyst (Table 2) suggests the predominance of bridged-bonded CO, in good accordance with infrared analysis and expected for low dispersed samples. For Pd-Cl and Pd-acac catalysts, a greater fraction of linear-bonded CO was obtained as expected on highly dispersed samples. However, the L_1/L_2 ratio was higher for the Pd-Cl catalyst. L_1/L_2 ratio can be seen as the relative proportion of Pd(1 0 0) and Pd(1 1 1) planes at the surface. Therefore, on the Pd-Cl catalyst the surface density of Pd(1 0 0) planes is larger than on the Pd-acac and Pd-N catalysts. This result agrees very well with the behavior observed in FTIR analyses.

During TPD analysis, CO_2 and H_2 evolved simultaneously to CO desorption, and their profiles are shown in Fig. 5. For Pd-Cl and Pd-acac catalysts, CO_2 formation occurred in two regions. In the first region, with peaks at 512 and 613 K for Pd-Cl catalyst and at 613 K for the Pd-acac catalyst, CO_2 formation is assigned to the CO disproportionation reaction ($2CO \rightarrow CO_2 + C_s$). Note that CO dissociated in greater extent and at lower temperature for the Pd-Cl catalyst. In the second region, with peaks at 751 and 773 K, respectively, for Pd-Cl and Pd-acac catalysts, CO_2 formation originates from the water gas-shift reaction ($CO + OH_s \rightarrow CO_2 + 1/2H_2$), since hydrogen is also formed. For the Pd-N catalyst, there was no disproportionation of CO and the whole CO_2 produced came from the shift reaction.

The absence of CO disproportionation for the Pd-N catalyst points out the effect of particle size in the CO–Pd interaction. Ichikawa et al. [44] have reported that on small particles CO dissociates into CO_2 and carbon, but not on large ones. TPD of CO adsorbed on Pd/SiO_2 catalysts carried out by Rieck and Bell [38] supports the observed behavior that CO_2 formation decreases as Pd particle size increases. The presence of low coordination sites with Pd(1 0 0) orientation on the Pd-Cl catalyst associated to its greater CO disproportionation at lower temperature suggest that the sites arrangement favor the dissociation of carbon monoxide. With a smaller atomic density and tetra-coordinated sites, Pd(1 0 0) sites affected the Pd–CO bond strength. Thus, one could think that bridged CO strongly bonded

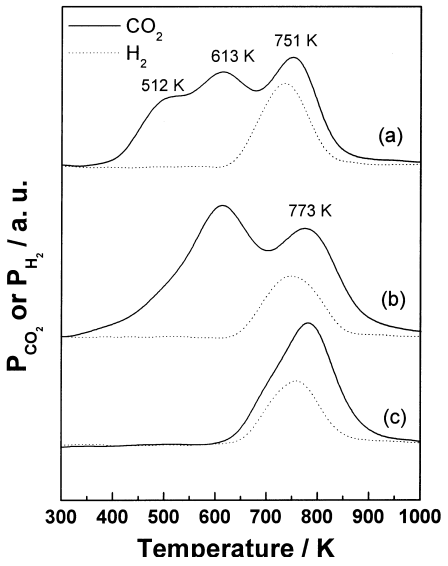

Fig. 5. CO_2 and H_2 evolution during TPD of Pd/Al_2O_3 catalysts: (a) Pd-Cl; (b) Pd-acac; and (c) Pd-N.

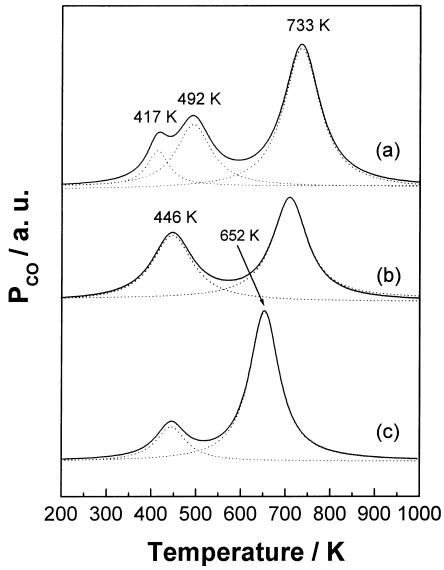

Fig. 6. TPD profiles for $Pd/CeO_2/Al_2O_3$ catalysts: (a) PdCe-Cl; (b) PdCe-acac; and (c) PdCe-N.

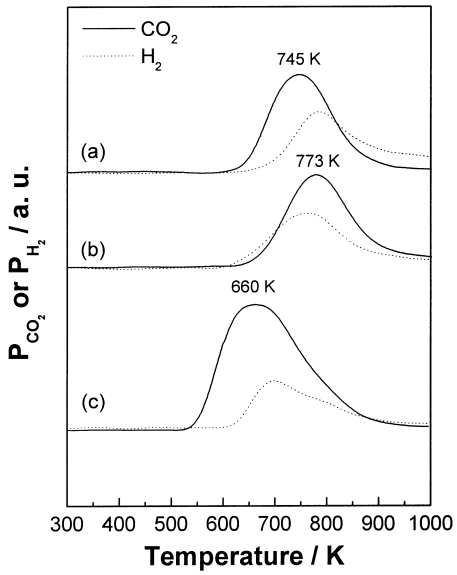

Fig. 7. CO_2 and H_2 evolution during TPD of $Pd/CeO_2/Al_2O_3$ catalysts: (a) PdCe-Cl; (b) PdCe-acac; and (c) PdCe-N.

would react with linear CO weakly bonded in adjacent sites to form CO_2 and carbon over Pd(1 0 0) surfaces.

The addition of CeO_2 significantly modified the CO profiles as well as the CO_2 formation during thermal desorption, as can be seen in Figs. 6 and 7, respectively. A strong decrease in the intensity of linear CO species was observed, being also affected by the distribution of L_1 and L_2 species (Table 2). For the PdCe-Cl catalyst, CO adsorbed on Pd(1 0 0) and Pd(1 1 1), respectively, at 417 and 492 K, showing up the same L_1/L_2 ratio of the Pd-Cl catalyst, but the desorption temperatures were slightly lower. For PdCe-acac and PdCe-N catalysts, CO adsorbed on Pd(1 0 0) faces was not observed, and their common peak at 446 K is attributed to linear-bonded CO on Pd(1 1 1) faces. This peak also desorbed at a lower temperature in comparison with the catalysts with no ceria. As a consequence of linear species partial suppression, the bridge-to-linear ratio (B/L) increased for PdCe-Cl and PdCe-acac catalysts. In turn, CO_2 formation observed during TPD (Fig. 7) originated only from the shift reaction. No CO disproportionation was recorded.

These results reinsure that Pd–Ce interaction influenced the Pd particle morphology in accordance with FTIR analyses. For the PdCe-Cl catalyst, the absence of a strong interaction due to the presence of chlorine ions on the surface has caused the growing of metallic particles altering the CO chemisorption stoichiometry. High coordination sites would be formed in a three-dimensional arrangement with a predominance of (1 1 1) faces. On this structure, CO would adsorb preferentially on a bridged-bonded form. Studies based on low dispersed Pd/SiO_2 catalysts showed that as the dispersion decreases the proportion of Pd(1 1 1) sites relative to Pd(1 0 0) sites increases with a decreasing of the amount of linear-bonded CO [38]. On the other hand, for PdCe-acac and PdCe-N catalysts, the epitaxial alignment between ceria vacancies and Pd crystallites favored the formation of Pd(1 1 1) surfaces with CO bonding in a bridge form.

The non-existence of CO disproportionation is also related to the modification of Pd nature sites due to their interaction with ceria. The decreasing of particle size on the PdCe-Cl catalyst would be behind this behavior since CO only dissociates on small particles. As mentioned earlier, Pd(1 0 0) faces promote CO dissociation due to its arrangement with low coordination sites. The presence of ceria appears to inhibit this crystallographic orientation resulting, therefore, in the suppression of CO dissociation.

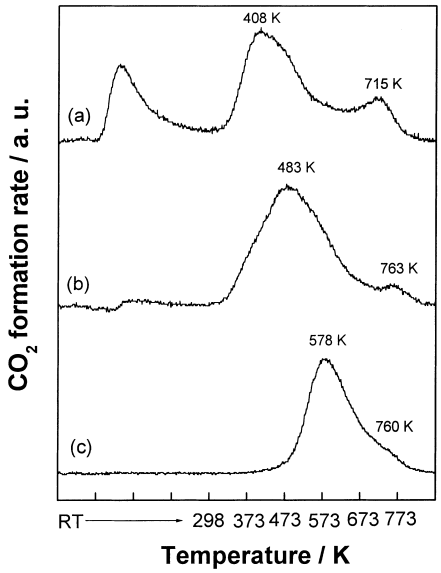

Fig. 8. TPSR profiles for Pd/Al_2O_3 catalysts: (a) Pd-Cl; (b) Pd-acac; and (c) Pd-N.

3.2. Unsteady-state oxidation of carbon monoxide

3.2.1. Pd/Al_2O_3 catalysts

Temperature-programmed surface reaction (TPSR) results for the Pd-Cl, Pd-acac and Pd-N catalysts are shown in Fig. 8. CO_2 evolved simultaneously to O_2 uptake and it was not observed in any desorption of CO during the reaction in these samples. For clarity's sake only the CO_2 profiles are presented. Mass balances of CO to CO_2 conversion and O_2 uptake are shown in Tables 3 and 4, respectively.

The formation of CO_2 was noticed only after an initial oxygen uptake at room temperature, which is related to the adsorption of the oxygen molecule. This lag is associated to the necessity of oxygen to adsorb firstly on the surface, which would then allow pre-adsorbed carbon monoxide to oxidize. The mechanism for CO oxidation involves the reaction between $CO_{ads.}$ and $O_{ads.}$, in accordance with the classical Langmuir–Hinshelwood kinetics described by Engel and Ertl [3,4]. An alternative to this assumption would be Eley–Rideal mechanism, which proposes that one of the reactants in the gas phase (O_2) would collide with the another reactant adsorbed ($CO_{ads.}$). This latter hypothesis is easily disregarded since only carbon dioxide evolved after oxygen chemisorption took place. However, a question to be raised is how did O_2 molecules adsorb in CO pre-saturated surfaces? The adsorption of O_2 is dissociative, occupying two adjacent sites, so a large surface area is needed. At least three possibilities can be proposed in order to explain oxygen adsorption.

First, CO displacement on a Pd saturated surface by O_2 leads to the formation of domains of CO and atomic oxygen adsorbed over a metallic surface. Second, CO molecules either desorb or migrate to the support through a spillover process. And third, CO would be displaced, but the subsequent activation of oxygen atom would also lead it to migrate to the support.

It is very reasonable to think that the first and third possibilities are the most likely processes, but it is hard

Table 3
Total mass balance from TPSR profiles

Sample	Amount (g)	n_{CO}[a] (μmol mg^{-1} Pd)	n_{CO_2}[b] (μmol mg^{-1} Pd)	Δ[c] (%)	n_{O_2}[d] (μmol mg^{-1} Pd)	n_{O_2}[e] (μmol mg^{-1} Pd)	n_{O_2}[f] (μmol mg^{-1} Pd)
Pd-Cl	0.2972	4.26	6.99	39	5.89	5.75	4.70
Pd-acac	0.2554	4.93	7.64	35	8.46	5.42	4.70
Pd-N	0.9482	1.06	1.73	39	2.45	6.20	4.70
PdCe-Cl	0.6720	2.13	3.19	33	13.01	16.04	4.70
PdCe-acac	0.2517	4.55	6.43	29	19.91	9.90	4.70
PdCe-N	0.5485	2.03	3.15	36	16.77	9.91	4.70

[a] CO (μmol) adsorbed by pulses.
[b] CO_2 (μmol) formed during TPSR analysis.
[c] Percentage deviation from stoichiometry to complete CO oxidation, given by $(n_{CO_2} - n_{CO})/n_{CO_2} \times 100$.
[d] O_2 uptake during TPSR analysis at room temperature.
[e] O_2 uptake during TPSR analysis from RT to 773 K.
[f] O_2 needed to complete oxidation of $Pd^0 \rightarrow PdO$.

Table 4
Total O_2 mass balance from TPSR profiles

Sample	$n_{O_2}(1) + n_{O_2}(2)$[a] (μmol mg^{-1} Pd)	$n_{CO_2}/2 + n_{O_2}(3)$[b] (μmol mg^{-1} Pd)	ε[c] (%)
Pd-Cl	11.64	8.20	30
Pd-acac	13.88	8.52	38
Pd-N	8.65	5.57	36
PdCe-Cl	29.05	6.30	78
PdCe-acac	29.81	7.92	73
PdCe-N	26.68	6.28	76

[a] Total O_2 uptake during TPSR analysis.
[b] Total O_2 needed stoichiometrically to oxidize CO and metallic Pd.
[c] Percentage deviation from the stoichiometry to oxidize completely CO and metallic Pd.

to discriminate between them and further experiments are necessary, beyond the scope of this work. One can imagine them happening simultaneously or in a complementary way. The second possibility seems to be more unlikely, because no CO desorption was observed, and at room temperature CO spillover should not easily occur.

Mass balance results presented in Tables 3 and 4 shows a percentage deviation ranging from 30 to 40% in relation to the stoichiometry of CO_2 formation as well oxygen uptake to oxidize completely CO and metallic palladium. Metallic palladium is another source for oxygen consumption, and TPO studies carried out by several authors [45,46] have reported that in the temperature herein used for TPSR experiments (673 K), palladium particles must be fully oxidized. However, as yet the oxygen uptake exceeds which is necessary, the occurrence of spillover cannot be disregarded.

Looking back again to the TPSR curves (Fig. 8), meaningful differences can be observed in the carbon monoxide oxidation activity. At room temperature (RT), an intense peak of CO_2 for Pd-Cl catalyst is observed, while for the Pd-acac catalyst a very small amount of CO_2 is noticed. No activity for the Pd-N catalyst at room temperature is observed. Higher rates for all catalysts were obtained at higher temperatures, but the maximum activities were sensibly temperature-dependent. A large peak at 408 K observed for Pd-Cl is shifted to 483 K for Pd-acac and 578 K for Pd-N catalysts. Furthermore, small shoulders above 700 K can also be seen for all catalysts following the same temperature-dependence behavior. By taking into account CO_2 formation at RT and the position of the most intense peaks at high temperatures, Pd/Al_2O_3 catalysts show the following activity pattern: Pd-Cl > Pd-acac > Pd-N.

Indeed, these results strongly suggest the influence of the precursors on the nature of Pd catalytic sites toward CO oxidation. Three distinct sites can be identified and their presence and activity appear to be determined by the precursors. As described earlier in the previous section, properties such as Pd particle size, support interaction, and site morphology changed as the Pd precursor salts changed as well, so different reactivities would then be expected to observe.

Despite that Pd-Cl and Pd-acac catalysts have presented the same metallic dispersion, they did not show site property equivalence as already shown by FTIR and TPD results. The larger amount of sites with low coordination on Pd(1 0 0) surfaces for the Pd-Cl catalyst could be associated to the higher rates of CO_2 formation at RT. On these sites, the lowest electron availability to back-donate to the $2\pi^*$-antibonding orbital of CO would weaken Pd–CO bond strength, which results in readiness of CO to easily oxidize at low temperatures. On the other side, the high coordination sites on Pd(1 1 1) surfaces, on which CO preferentially bonded in bridged, strengthened the Pd–CO bond. Thus, on these sites CO oxidation is expected to occur at higher temperatures and in fact it was observed for both the Pd-acac and Pd-N catalysts.

According to Pavlova and Sadykov [6,7] and Kochubey et al. [47] small metallic ensembles of Pd supported on SiO_2, TiO_2 and Al_2O_3 have presented unlike morphology and distribution, with the presence of distorting Pd surface structures and lots of defects where CO and O_2 adsorption were observed. Weakly bonded linear and bridged CO species were the most reactive species, being located preferentially on flaw

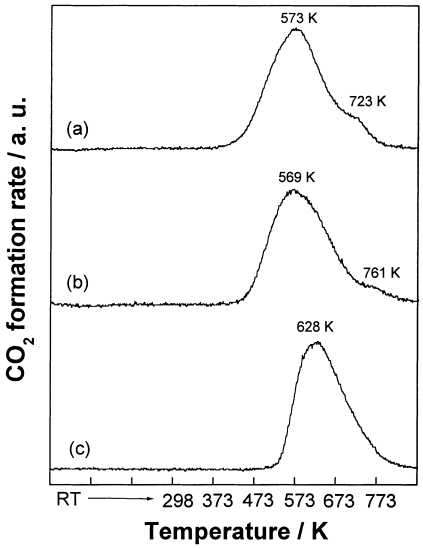

Fig. 9. TPSR profiles for $Pd/CeO_2/Al_2O_3$ catalysts: (a) PdCe-Cl; (b) PdCe-acac; and (c) PdCe-N.

sites of (1 0 0) or (1 1 0) orientation. In these samples, CO oxidation was structure sensitivity at low temperatures, and the reaction occurred via interaction of weakly bonded CO with oxygen in adjacent sites [6].

3.2.2. $Pd/CeO_2/Al_2O_3$ catalysts

Fig. 9 shows TPSR results for the PdCe-Cl, PdCe-acac and PdCe-N catalysts. Similar the behavior observed in their counterparts without ceria, CO_2 evolved simultaneously during O_2 uptake and it was not observed in any desorption of CO under reaction. An enormous oxygen uptake at room temperature was observed for these catalysts. Considering the presence of ceria reduced species (Ce^{3+}), the greater part of the consumption of oxygen is assigned to oxidation of the CeO_x species to CeO_2.

There was no observation of any formation of CO_2 at room temperature. PdCe-Cl and PdCe-acac catalysts showed very similar profiles with a CO_2 peak formation around 570 K and a shoulder higher than 700 K. For the PdCe-N catalyst, CO oxidation occurred at higher temperatures with only a broad peak at 628 K. Comparing these results with those obtained for the catalysts with no ceria, it is noteworthy that the oxidation of CO occurred at higher temperatures. It evidences that the Pd–Ce interaction previously characterized played no promotional role in the CO oxidation activity.

The presence of CeO_2 is expected to promote the CO oxidation through the reaction between adsorbed CO and oxygen from its lattice [48]. Ceria promotion consists of suppressing the CO inhibition effect in the adsorption rates of oxygen. Therefore, the inverse first-order dependence on CO concentration is eliminated because ceria supplies the oxygen needed to oxidize CO. However, the beneficial effect of ceria reported in the literature has been observed in steady-state conditions with the reaction rates measured in a range of partial pressures of CO and O_2 [49,50].

In this study, unsteady-state conditions were used, and one of the reactants (CO) was previously adsorbed on reduced samples, which meant that oxygen-deficient vacancies on ceria lattice should be present. Therefore, one can imagine that most of the oxygen uptake during TPSR analysis went directly to replenish the ceria oxygen-deficient lattice, instead of oxidizing CO. There would then be a fierce competition between the CeO_x species and Pd sites by the molecule of oxygen. Thus, oxygen would be available to CO oxidation only after complete reoxidation of ceria reduced species. This behavior could be one of the reasons in not observing CO oxidation at low temperatures.

On the other hand, the increase of bridged-bonded CO on high coordination sites on Pd(1 1 1) surfaces, as a consequence of Pd–Ce interaction, would also contribute to a shift in CO oxidation to higher temperatures. This surface configuration strengthens the Pd–CO bond and higher temperatures would be needed to compress CO molecules for allowing oxygen to adsorb on Pd sites. Thus, a combination of strong competition for O_2 molecules and low activity of Pd sites would increase the temperature for CO oxidation on $Pd/CeO_2/Al_2O_3$ catalysts.

4. Conclusions

The role of palladium precursors in the catalytic properties toward CO oxidation for Pd/Al_2O_3 and $Pd/CeO_2/Al_2O_3$ catalysts was investigated in this study. Pd(1 0 0) and Pd(1 1 1) were the major palladium crystallite orientations in these samples, and the distribution and proportion of such surfaces were affected by the Pd precursor nature and the presence

of CeO_2. Highly dispersed metal particles obtained by using palladium chloride and acetylacetonate precursors were the most active sites in CO oxidation. On these surfaces, the greater amount of low coordination sites on Pd(1 0 0) faces was responsible for the good activity observed at very low temperatures.

In the presence of ceria, the existence of an epitaxial alignment between ceria anionic vacancies and Pd dispersed crystallites changed the Pd sites nature. In these catalysts, Pd(1 1 1) faces were favored in detriment of Pd(1 0 0) faces. Furthermore, due to the transient conditions carried out in this study, ceria did not promote, as expected, the oxidation of CO. Ceria reduced species (Ce^{3+}) were not able to help CO to oxidize due to lack of oxygen in its lattice. Thus, the highest rates of CO oxidation were only observed at higher temperatures as a result of a combination of strong competition for oxygen molecules and low activity of Pd(1 1 1) sites.

Acknowledgements

The authors would like to acknowledge Ruth L. Martins, Leila Merat, Sidnei Joaquim and Victor T. Santos for technical support during the characterization work. One of the authors (R.S. Monteiro) would like to thank CAPES (Ministry of Education, Brazil) for financial aid.

References

[1] B. Harrison, A.F. Diwell, C. Hallett, Plat. Met. Rev. 32 (1988) 73.
[2] M. Jacoby, Chem. Eng. News 77 (1999) 36.
[3] T. Engel, G. Ertl, J. Chem. Phys. 69 (1978) 1267.
[4] T. Engel, G. Ertl, Adv. Catal. 28 (1979) 1.
[5] M. Haruta, S. Tsubota, T. Kobayashi, H. Kageyama, M.J. Genet, B. Delmon, J. Catal. 144 (1993) 175.
[6] S.N. Pavlova, V.A. Sadykov, V.A. Razdobarov, E.A. Paukshtis, J. Catal. 161 (1996) 507.
[7] S.N. Pavlova, V.A. Sadykov, N.N. Bulgakov, M.N. Bredikhin, J. Catal. 161 (1996) 517.
[8] G.A. Somorjai, Introduction to Surface Chemistry and Catalysis, Wiley, New York, NY, 1994, p. 442.
[9] M. Alexandrou, R.M. Nix, Surf. Sci. 321 (1994) 47.
[10] M.G. Sanchez, J.L. Gazquez, J. Catal. 104 (1987) 120.
[11] S. Bernal, J.J. Calvino, M.A. Cauqui, J.M. Gatica, C. Larese, J.A. Perez Omil, J.M. Pintado, Catal. Today 50 (1999) 175.
[12] J.A.R. Rob van Veen, G. Jonkers, H. Hesselink, J. Chem. Soc., Faraday Trans. 1 85 (1989) 389.
[13] R.S. Monteiro, C.L. Araujo, C.A. Perez, H.S. Amorim, M. Schmal, L.C. Dieguez, XVI Simposio Iberoamericano de Catalisis, Cartagena de Indias, Colombia, 1998, p. 2237.
[14] M.F.L. Johnson, J. Mooi, J. Catal. 103 (1987) 502.
[15] V. Perrichon, A. Laachir, G. Bergeret, R. Frety, L. Tournayan, O. Touret, J. Chem. Soc., Faraday Trans. 90 (1994) 773.
[16] L.G. Appel, J.G. Eon, M. Schmal, Catal. Lett. 56 (1998) 199.
[17] J.E. Benson, H.S. Hwang, M. Boudart, J. Catal. 30 (1973) 146.
[18] D.J.C. Yates, J.H. Sinfelt, J. Catal. 8 (1967) 348.
[19] H. Lieske, G. Lietz, H. Spindler, J. Völter, J. Catal. 81 (1983) 8.
[20] H. Lieske, J. Völter, J. Phys. Chem. 89 (1985) 1841.
[21] D.O. Simone, T. Kennelly, N.I. Brungard, R.J. Farrauto, Appl. Catal. 70 (1991) 87.
[22] R.S. Monteiro, F.B. Noronha, L.C. Dieguez, M. Schmal, Appl. Catal. A: General 131 (1995) 89.
[23] A.K. Datye, D.S. Kallakkad, M.H. Yao, D.J. Smith, J. Catal. 155 (1995) 148.
[24] D.S. Kalakkad, A.K. Datye, H.J. Robota, J. Catal. 148 (1994) 729.
[25] F. Le Normand, L. Hilaire, K. Kili, G. Krill, G. Maire, J. Phys. Chem. 92 (1988) 2561.
[26] K. Kili, F. Le Normand, J. Mol. Catal. A: Chemical 140 (1999) 267.
[27] F. Fajardie, J.-F. Tempere, J.-M. Manoli, G. Djega-Mariadassou, G. Blanchard, J. Chem. Soc., Faraday Trans. 94 (1998) 3727.
[28] L. Kepinski, M. Wolcyrz, J. Sol. Stat. Chem. 131 (1997) 121.
[29] D.I. Kondarides, X.E. Verykios, J. Catal. 174 (1998) 52.
[30] R.P. Eischens, W.A. Pliskin, Adv. Catal. 10 (1958) 1.
[31] R.R. Ford, Adv. Catal. 21 (1970) 51.
[32] A. Palazov, C.C. Chang, R.J. Kokes, J. Catal. 36 (1975) 338.
[33] G. Blyholder, J. Phys. Chem. 68 (1964) 2772.
[34] A.M. Bradshaw, F.M. Hoffmann, Surf. Sci. 72 (1978) 513.
[35] A. Ortega, F.M. Hoffman, A.M. Bradshaw, Surf. Sci. 119 (1982) 79.
[36] A. Palazov, G. Kadinov, C. Bonev, D. Shopov, J. Catal. 74 (1982) 44.
[37] D. Tessier, A. Rakai, F. Bozon-Verduraz, J. Chem. Soc., Faraday Trans. 88 (1992) 741.
[38] J.S. Rieck, A.T. Bell, J. Catal. 103 (1987) 46.
[39] J.Z. Shyu, K. Otto, W.L.H. Watkins, G.W. Graham, R.K. Belitz, H.S. Gandhi, J. Catal. 114 (1988) 23.
[40] A.S. Sass, V.A. Shvets, G.A. Savel'eva, N.M. Popova, V.B. Kazanskii, Kinet. Catal. 27 (1986) 777.
[41] A. Badri, C. Binet, J.-C. Lavalley, J. Chem. Soc., Faraday Trans. 92 (1996) 1603.
[42] J.L. Duplan, H. Praliaud, Appl. Catal. 67 (1991) 325.
[43] J.S. Rieck, A.T. Bell, J. Catal. 96 (1985) 88.
[44] S. Ichikawa, H. Poppa, M. Boudart, J. Catal. 91 (1985) 1.
[45] T.E. Hoost, K. Otto, Appl. Catal. A: General 92 (1992) 39.
[46] Y.L. Lam, M. Boudart, J. Catal. 47 (1977) 393.
[47] D.I. Kochubey, S.N. Pavlova, B.N. Novgorodov, G.N. Kryukova, V.A. Sadykov, J. Catal. 161 (1996) 500.
[48] T. Jin, Y. Zhou, G.J.M. Mains, J.M. White, J. Phys. Chem. 91 (1987) 5931.
[49] S.H. Oh, C.C. Eickel, J. Catal. 112 (1988) 543.
[50] Y.-F. Yu Yao, J. Catal. 87 (1984) 152.